

Dalton Transactions

Accepted Manuscript



This is an *Accepted Manuscript*, which has been through the Royal Society of Chemistry peer review process and has been accepted for publication.

Accepted Manuscripts are published online shortly after acceptance, before technical editing, formatting and proof reading. Using this free service, authors can make their results available to the community, in citable form, before we publish the edited article. We will replace this *Accepted Manuscript* with the edited and formatted *Advance Article* as soon as it is available.

You can find more information about *Accepted Manuscripts* in the [Information for Authors](#).

Please note that technical editing may introduce minor changes to the text and/or graphics, which may alter content. The journal's standard [Terms & Conditions](#) and the [Ethical guidelines](#) still apply. In no event shall the Royal Society of Chemistry be held responsible for any errors or omissions in this *Accepted Manuscript* or any consequences arising from the use of any information it contains.



www.rsc.org/dalton

Spectroscopic signatures of ligand field states in {Ru^{II}(imine)} complexes

Alejandro Cadranel,[†] German E. Pieslinger,[†] Pornthip Tongying,[‡]

Masaru K. Kuno,[‡] Luis M. Baraldo,[†] José H. Hodak.^{†*}

[†] Departamento de Química Analítica, Inorgánica y Química Física, INQUIMAE, Facultad de Ciencias Exactas y Naturales, Universidad de Buenos Aires, Pabellón 2, Ciudad Universitaria, C1428EHA, Buenos Aires, Argentina.

[‡] Department of Chemistry and Biochemistry, University of Notre Dame, Notre Dame, Indiana 46656, United States.

Abstract

Ligand field (LF) states have been present in discussions on the photophysics and photochemistry of ruthenium-iminic chromophores for decades, although there is very little documented direct evidence of them. We studied the picosecond transient absorption (TA) spectroscopy of four {Ru^{II}(imine)} complexes that respond to the formula *trans*-[Ru(L)₄(X)₂], where L is either pyridine (py) or 4-methoxypyridine (MeOpy) and X is either cyanide or thiocyanate. Dicyano compounds behave as most ruthenium polypyridines and their LF states remain silent. In contrast, in the dithiocyanate complexes we found clear spectroscopic evidence of the participation of LF states in the MLCT decay pathway. These states are of donor and acceptor character simultaneously and this is manifested in the presence of MLCT and LMCT transient absorption bands of similar energy. Spectroelectrochemical techniques supported the interpretation of the absorption features of MLCT states, and DFT methods helped to assign their spectroscopic signatures and provided strong evidence on the nature of LF states.

Keywords

Ligand Field States – dd states – metal centered states – ruthenium tetrapyridine – ruthenium tetrakispyridine – ultrafast spectroscopy

Introduction

The family of {Ru^{II}(imine)} complexes is one of the most frequent platforms chosen to study the photochemical and photophysical properties of coordination compounds.^{1–4} After decades of research, these compounds serve as models and are also playing crucial roles in photocatalysis,^{5–10} dye-sensitized solar cells,^{11–16} sensors^{17–21} and drug delivery.^{22,23} Their unique properties arise from the balance between metal-to-ligand charge transfer (MLCT) and ligand field (LF) excited states, although LLCT, MMCT and other states are sometimes involved.²⁴ The MLCT manifold of excited states, formally described as {Ru^{III}(imine⁻)} fragments, can be accessed from the ground state through intense and tunable light absorption.²⁵ These excited states are themselves highly absorbing, and usually photoluminescent. This facilitated extensive studies of their photophysical behavior through different spectroscopic techniques.²⁶ LF states have also been involved in discussions on ruthenium-iminic chromophores for over four decades.^{27–32} Generally, in these complexes LF states are energetically higher than MLCT states, although they are thermally accessible. Their electronic configuration can be described as $(t_{2g})^5(e_g)^1$ in an octahedral environment, and thus they are also known as *dd* states. Population of the antibonding e_g orbital significantly enlarges metal-ligand distances, favoring non-radiative decay to the ground state and also dissociative processes.^{29,33} Thus, LF states are avoided for photovoltaic applications, although they are targeted with analytical³⁴ or medical³⁵ purposes. In one sense or the other, control over these states is a major concern in all these applications.

In $\{\text{Ru}^{\text{II}}(\text{imine})\}$ compounds LF states have been typically addressed indirectly, through temperature-dependent photoluminescence measurements, and they have found to effectively quench MLCT at different temperatures depending on their accessibility.^{29,33} Further indirect evidence of the presence of LF states was documented by Hewitt et al., who suggested excited-state equilibration based on a loss of MLCT intensity in transient absorption measurements.³⁶ Recently, Sun and coworkers estimated transient absorption features which they ascribed to the LF manifold through singular value decomposition of their data in ultrafast experiments.³⁷ However, since $\{\text{Ru}^{\text{II}}(\text{imine})\}$ LF states are non-emissive and short-lived,^{29,33} they remained elusive of direct measurements.

Here we present a case where the usually silent LF states show themselves through clear transient absorption signatures. We focused on a series of *trans*- $[\text{Ru}(\text{L})_4(\text{X})_2]$ chromophores, where L is either pyridine (py) or 4-methoxypyridine (MeOpy) (see Figure 1) and X is either cyanide or thiocyanate. These complexes were selected because they have high energy MLCT states, proper of ruthenium tetrapyridines.^{38,39} From the initial MLCT state, internal conversion to the LF manifold may result an exergonic process, allowing for an increased rate of population of these metal centered states and their spectroscopic detection. In other $\{\text{Ru}^{\text{II}}(\text{imine})\}$ complexes with lower MLCT states, this process is uphill and thermally activated, thus hardly reaching sufficiently high populations of LF states to enable the detection of their spectroscopic signatures.²⁹ The *trans*- $[\text{Ru}(\text{L})_4(\text{X})_2]$ are expected to present LF states with different accessibility, given the different positions of CN^- and NCS^- in the spectrochemical series. Furthermore, in comparison with the vast majority of reported $\{\text{Ru}(\text{imine})\}$ complexes, the blue-shift in the ground state absorption features of *trans*- $[\text{Ru}(\text{L})_4(\text{X})_2]$ result in cleaner transient absorption spectra in the 400-700 nm region. It

is this judicious combination of factors that enabled us for the first time to directly detect UV-visible spectral signatures of LF states in $\{\text{Ru}^{\text{II}}(\text{imine})\}$ complexes. Picosecond transient absorption spectroscopy experiments were conducted to probe their excited state dynamics. Interpretation of the absorption features of MLCT states is based on spectroelectrochemical experiments, and DFT calculations provide strong evidence that help to identify the spectroscopic signatures of LF excited states.

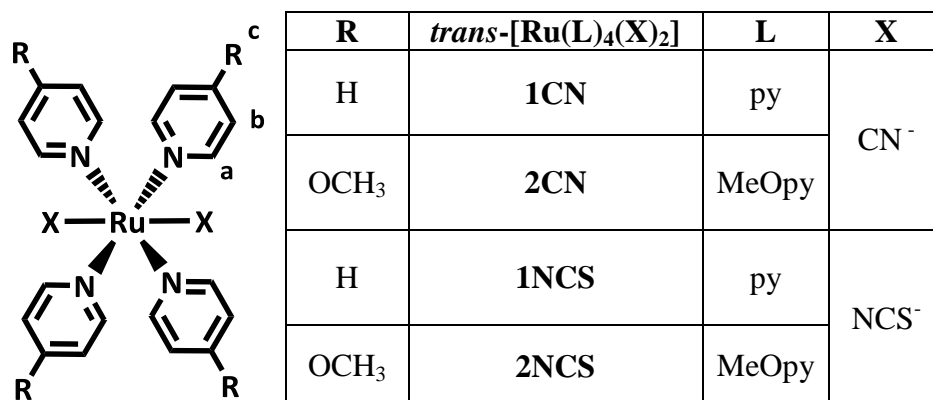


Figure 1. Sketches of the complexes $[\text{Ru}(\text{L})_4(\text{X})_2]$ reported in this work. Alphabetic

labels identify H atoms according to NMR assignments.

Results and Discussion

Crystal structures

Slow evaporation of a solution of **2NCS** in acetonitrile rendered single crystals suitable for X-ray diffraction measurements. This technique gave access to the crystal structure of complex **2NCS** (Figure 2), whose selected bond distances and angles are summarized in Table 1. Some distances and angles appear duplicated because the crystal structure presents a C_2 symmetry axis that contains the metal ion. **1-2CN** and **1NCS** have already been characterized by X-ray diffraction.^{39–41}

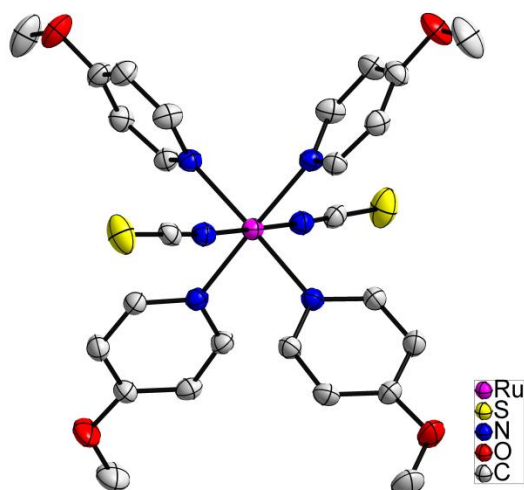


Figure 2. X-ray structure of complex **2NCS**. Ellipsoids represent a 30% displacement probability. Hydrogen atoms were omitted for clarity.

2NCS	
Distances / Å	Angles / °
Ru-N_{NCS}	Ru-N-C_{NCS}
2.035(4)	171.6(4)
2.035(4)	171.6(4)
N-C_{NCS}	N-C-S
1.156(6)	179.2(4)
1.156(6)	179.2(4)
C-S	N_{NCS}-Ru-N_{NCS}
1.638(6)	179.4(2)
1.638(6)	
Ru-N_{py}	
2.092(3)	
2.092(3)	
2.090(3)	
2.090(3)	

Table 1. Selected bond distances and angles for **2NCS**.

In **2NCS**, the ruthenium ion presents a nearly octahedral coordination sphere of nitrogen atoms. Pyridines are disposed in the typical propeller-like configuration of ruthenium tetrakis(pyridinic) fragments, and Ru-N_{py} bond lengths (~2.091 Å) are similar to those found in similar compounds.^{39,41–43} Importantly, the N coordination of NCS⁻ is confirmed. The thiocyanate ligands retain the linearity found in their free form (N-C-S angles >179°). In comparison with the parent compound [Ru(py)₄(NCS)₂], **2NCS**

displays shorter Ru-N-C_{NCS} angles (171.6° vs 175.6°) and longer Ru-N_{NCS} distances (2.035 Å vs 2.025 Å),⁴⁰ suggesting a poorer π -backbonding interaction and a slightly weaker bond in **2NCS**. Thiocyanate ligands are arranged in a *trans* fashion, with a N_{NCS}-Ru-N_{NCS} angle of 179.4°.

Electrochemistry

Comp.	$E_{1/2} (\Delta E_p)/V$ (mV) ^a	
	Ru(III/II)	L/L ⁻
1CN	0.85 (70) ^b	-2.26 ^d
2CN	0.67 (70) ^c	-2.53 ^d
1NCS	0.69 (80)	-2.23 ^d
2NCS	0.56 (100)	-2.55 ^d

Table 2. Electrochemical data for **1-2CN** and **1-2NCS** in acetonitrile. ^a 0.1 M [TBA]PF₆ used as electrolyte. ^b from reference ³⁹. ^c from reference ⁴¹. ^d irreversible.

Cyclic voltammograms of complexes **1-2NCS** are shown in Figures S1-2, and the resulting half wave reduction potentials are collected in Table 2. Anodic scans exhibit fully-reversible one-electron waves below 1 V, that resemble those previously reported for **1-2CN**.^{39,41} and thus they can be ascribed to Ru-centered couples. Within both families **1-2CN** and **1-2NCS**, their potential decreases as the substituted pyridine becomes a stronger σ -donor or a poorer π -acceptor. It was found that in any pair of compounds bearing the same pyridyl ligands, substitution of cyanide with thiocyanate results in a cathodic shift of the Ru(III/II) couple. This behavior results from the contrasting properties of the electron density acceptor CN⁻ and the donor NCS⁻. Unlike {Ru(bpy)₂(NCS)₂} analogues, **1NCS** and **2NCS** do not show any evidence of additional oxidation processes up to 1.5 V, which are usually ascribed to thiocyanate-centered processes.⁴⁴⁻⁴⁶ Furthermore, we found no evidence of decomposition upon one-electron oxidation. Cathodic scans show irreversible waves below -2 V, associated to

heterocyclic-centered reduction processes.⁴⁷ As expected, the enhanced electron richness of methoxy-substituted pyridines results in a more negative reduction potential.

UV-vis Spectroelectrochemistry

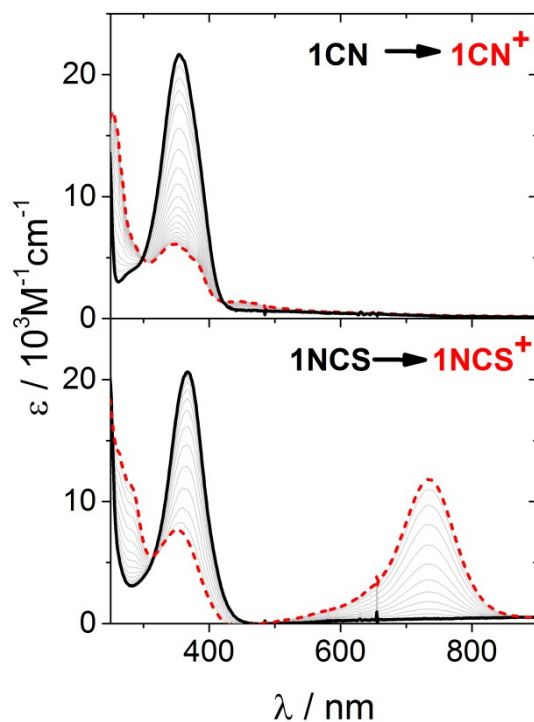


Figure 3. Oxidative spectroelectrochemistry of **1CN** and **1NCS** in methanol. Black solid curves are the initial spectra, and red dashed curves are the final ones. Grey lines indicate the spectral evolution.

Comp.	$\lambda_{\max} / \text{nm}$ ($\epsilon_{\max} / 10^3 \text{ M}^{-1} \text{ cm}^{-1}$)	
	MLCT $d\pi(\text{Ru}) \rightarrow \pi^*(\text{L})$	LMCT $\pi(\text{L}) \rightarrow d\pi(\text{Ru})$ $\pi(\text{X}) \rightarrow d\pi(\text{Ru})$
1CN	354 (21.7)	-
2CN	340 (20.6)	-
1CN⁺	-	349 (6.1) 448 (1.4)
2CN⁺	-	461 (9.9)
1NCS	370 (20.5)	-
2NCS	352 (22.4)	-
1NCS⁺	-	353 (7.7) 736 (11.9)

2NCS⁺	-	349 (3.7) (sh) 689 (14.2)
-------------------------	---	------------------------------

Table 3. Spectroscopic data for **1-2CN**, **1-2NCS** and their one-electron oxidized species in methanol.

Figures 3 and S3 present the absorption spectra of **1-2CN** and **1-2NCS**, and their evolution upon one-electron oxidation. Table 3 collects the relevant spectroscopic data. The $d\pi(\text{Ru}) \rightarrow \pi^*(\text{L})$ MLCT bands govern the absorption profiles of all the compounds reported here involving a Ru(II) oxidation state, with maxima in the range of 340-370 nm. For compounds with equal axial substitution, these bands shift to the blue as the iminic ligands are more electron-rich and harder to reduce. This effect overcomes the differences in the metal center reduction potentials. Additionally, for every pair of compounds bearing the same pyridinic ligand, MLCT band maxima shift to the red when CN^- is replaced by NCS^- . This tracks the differences in the reduction potentials of the metal couples and reflects the donor effect of the NCS^- ligands, which usually destabilizes HOMOs.⁴⁸

In both series **1-2CN** and **1-2NCS**, MLCT bands disappear upon one-electron oxidation (Figure 3), as expected for a process that depletes Ru(II) donors. Simultaneously, new signals of LMCT character grow for the dicyano- and dithiocyanato- complexes due to the presence of a Ru(III) acceptor. In **1-2NCS⁺** complexes, intense bands appear above 680 nm and shift to the blue upon decreasing the reduction potential of the metal couples, i.e. upon rising the energy of the acceptor Ru *d* orbitals. These observations strongly suggest that the NCS^- ligands are the origin of LMCT transitions, i.e. these correspond to $\pi(\text{NCS}) \rightarrow d\pi(\text{Ru})$.⁴⁹⁻⁵² The higher energy LMCT signals show almost no shift between **1NCS** and **2NCS** (both signals appear around 350 nm for both), so their assignment is discussed below on the basis of (TD)DFT techniques (*vide infra*). In contrast, in **1-2CN⁺** LMCT bands (448 nm and 461

nm with L = py and MeOpy, respectively) shift in the opposite direction, suggesting that for these compounds the $\pi(L)$ orbitals are involved in these bands. As observed for the MLCT bands of the non-oxidized species, when orbitals of both pyridines and the metal center are taking part in a charge transfer, the properties of the former dominates the energy trend. Such is the case of LMCT bands of **1-2CN**⁺. The oxidation processes for all the samples proceeded with retention of clear isosbestic points, which rules out decomposition upon one electron oxidation in the timescale of the spectroelectrochemical experiment. This result contrasts with the reports for other ruthenium dithiocyanate complexes,⁴⁴ except for [Ru(MeObpy)₂(NCS)₂] (MeObpy is 4,4'-methoxy-2,2'-bipyridine).⁴⁸

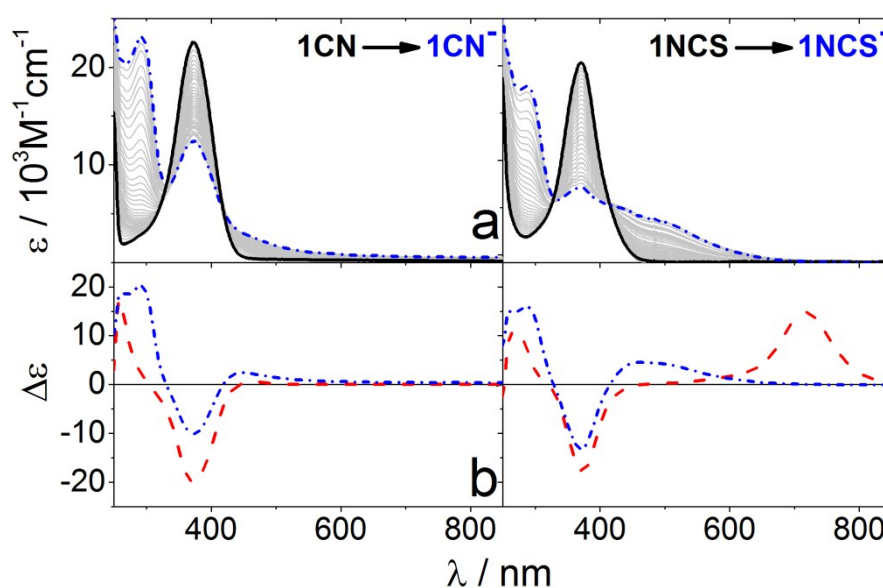


Figure 4. a) Reductive spectroelectrochemistry in acetonitrile of **1CN** (left) and **1NCS** (right). b) Difference spectra of the oxidation (dashed) and reduction (dash-dotted) processes of **1CN** (left) and **1NCS** (right).

Spectroelectrochemical studies during ligand reduction were also performed for **1CN** and **1NCS** (Figure 4). Full depletion of **1CN** and **1NCS** species was precluded by

solvent discharge at the negative end of the experimentally available electrochemical window in acetonitrile. For the same reasons, measurements for **2CN** and **2NCS** are unreliable due to the extremely high cathodic potential required for their reduction processes (Table 2) and will not be further discussed here. Upon reduction, MLCT bands decrease and several new signals grow (Figure 4). The intense new features around 290 nm and the broad signals over 430 nm can be assigned to $\pi^* \rightarrow \pi^*(L)$ intraligand transitions.^{48,53} Some contributions to absorption of the reduced species in the red flank of the MLCT band can be attributed to a red-shifted MLCT, which stems from destabilization of ruthenium *d* orbitals by the enhanced electron density on the reduced ligand.^{54,55}

The charge-separated nature of MLCT excited states allows their description as a simultaneously metal-oxidized and ligand-reduced species. Thus, the sum of the oxidative difference spectra of **1CN** and **1NCS** with their reductive difference spectra (Figure 5a) is a good starting point to analyze the transient absorption profile of the MLCT excited state. However, it must be kept in mind that this approach neglects the spectroscopic consequences of having a reduced ligand and an oxidized metal center simultaneously.^{53,56,57}

Transient absorption measurements

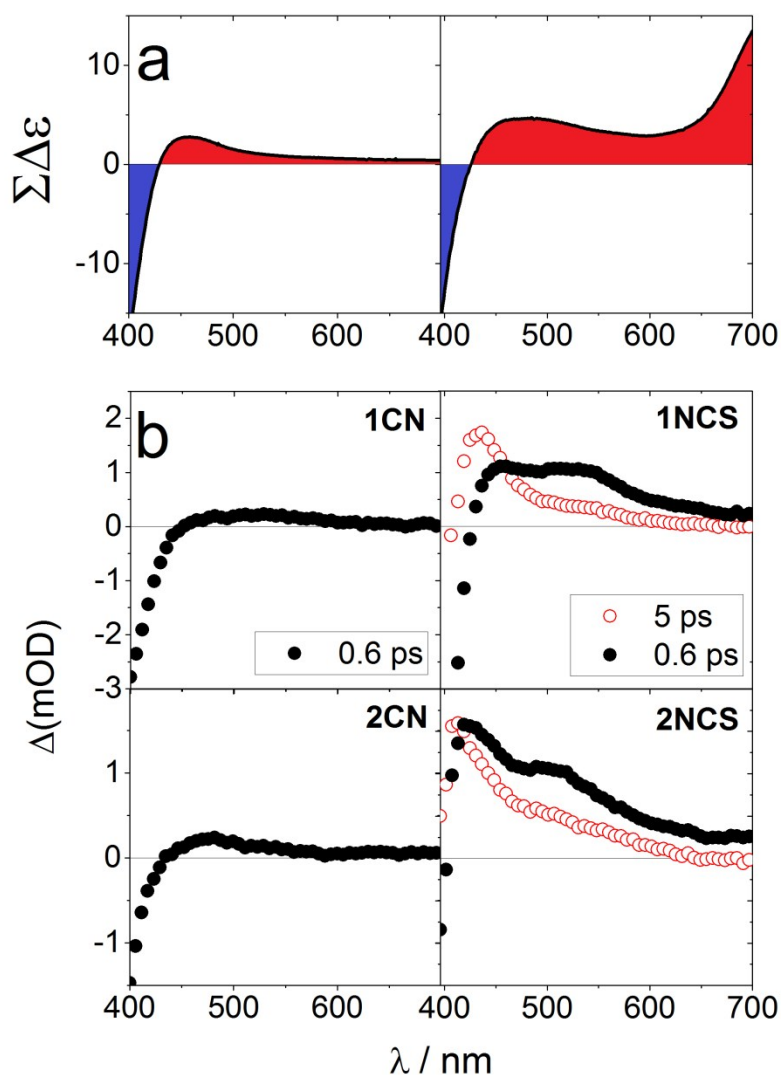


Figure 5. a) Sum of the oxidation and reduction difference spectra of **1CN** (left) and **1NCS** (right). b) Transient absorption spectra of **1-2CN** and **1-2NCS** in methanol, pumped at 387 nm.

All the complexes explored here are non emissive in thoroughly argon-degassed solutions in methanol at room temperature. This is the usual case for the $\{\text{Ru}(\text{py})_4\}$ core, and one of the reasons why so little is known about their excited states dynamics. Transient absorption measurements were performed to shed light on the dynamics of the MLCT excited states of **1-2CN** and **1-2NCS**. All the samples were pumped at 387 nm, in the red side of their MLCT absorption band (Figures 3 and S3). Figure 5 shows the

transient absorption spectra of compounds **1-2CN** and **1-2NCS**. For the analysis of these data, it was assumed that inter-system crossing between singlet and triplet MLCT manifolds occurs in around 50 fs, a timescale much faster than the resolution of our experiment.^{58,59} Hence, our interpretation starts with considering an initial ³MLCT population in the excited state.

Absorption profiles of the dicyano complexes 0.6 ps after excitation are essentially equal to each other, and remarkably similar to those predicted for **1CN** by spectroelectrochemical techniques (Figure 5). They display negative signals below 450 nm, which mirror the ground state MLCT absorption bands and can thus be ascribed to their bleaching. Also, low intensity broad positive signals can be distinguished around 500 nm. We assign them as $\pi^* \rightarrow \pi^*(L)$ intraligand transitions and $\pi^*(L) \rightarrow d\pi(\text{Ru})$ involving a semi-occupied π^* orbital of the reduced pyridine ligand, by comparison to our spectroelectrochemical experiments (Figure 5a) and analogous systems containing a $\{\text{Ru}(\text{bpy})_2\}$ fragment.^{48,60,61} These transient absorption characteristics resemble those of MLCT excited states in ruthenium polypyridyl complexes.^{53,56,57,62–64} In the case of **2CN**, it is worth to note the absence of contributions from $\pi(\text{MeOpy}) \rightarrow d\pi(\text{Ru})$ LMCT band proper of **2CN**⁺, expected around 460 nm (Figure S3). This intense and narrow signal might be considerably blue-shifted in the excited state, as a consequence of ruthenium *d* orbitals destabilization in the presence of a pyridinic radical anion ligand.

Both **1-2CN** exhibit a monoexponential decrease in the intensity of their transient absorption spectra as the only dynamics, without noticeable spectral shifts, and lifetimes of 8.6 and 7.1 ps for **1CN** and **2CN** respectively (Table 4). Kinetic traces for **1CN** and **2CN** have the same behavior (Figures 6 and S9) all through the explored spectral window, suggesting the loss of ³MLCT population is associated with ground state recovery.

The photophysical scenario of **1-2NCS** is remarkably different (Figure 5b). Absorption spectra of dithiocyanate complexes 0.6 ps after excitation can be assigned to $^3\text{MLCT}$ state as they show the features expected from the spectroelectrochemical experiments (Figure 5a): bleaching bands below 450 nm that mirror the ground state MLCT absorption, and a wide positive signal that extend to the red side of the visible spectrum. We assign them as a superposition of $\pi^*(\text{L}) \rightarrow d\pi(\text{Ru})$ and $\pi(\text{NCS}) \rightarrow d\pi(\text{Ru})$ LMCT transitions. As in related $\{\text{Ru}(\text{NCS})_2\}$ motifs,^{50,51} $\pi(\text{NCS}) \rightarrow d\pi(\text{Ru})$ LMCT absorption band of the $^3\text{MLCT}$ excited state is blue-shifted in comparison with the LMCT band of the one-electron oxidized species (Figures 3 and S3, and Table 3). This is a consequence of the presence of a radical anion pyridine ligand in the MLCT excited state, which destabilizes the ruthenium d orbitals.

Five ps after excitation, the transient absorption spectrum of **1NCS** presents clearly distinctive features (Figure 5b). The photoinduced bleach signal below 430 nm gradually turns into an absorption band in the range 410-480 nm (Figure 6) before complete recovery of the ground state. This biphasic behavior reveals the participation of an additional excited state in the decay pathway. In **2NCS** this behavior is also present, although is less pronounced due to the blue-shift of its spectral features.

We consider two alternatives for the nature of the process giving raise to this second excited state (**ES2**). One option is the linkage isomerization of the thiocyanate ligand in the $^3\text{MLCT}$ excited state, from the N-bound to S-bound, which then reverts to a N-bound ground state concomitantly with ground state recovery. In this picture, the **ES2** could be described as $\{\text{Ru}^{\text{III}}(\text{L})(\text{SCN})\}$. However, the absence of a dominating bleach signal (Figure 5b) strongly points to a Ru(II) character of the metal ion in this state. Furthermore, in contrast to sulfoxide Ru complexes,⁶⁵⁻⁷² the occurrence of such process has not been observed in iminic ruthenium thiocyanato complexes.^{48,73,74}

Additionally, TD(DFT) calculations (Figures S27 and S28) predict very similar absorption features for the three possible isomers (N,N-bound, N,S-bound and S,S-bound), suggesting a $\{\text{Ru}^{\text{II}}(\text{L})(\text{SCN})\}$ description of **ES2** could neither account for the photoinduced absorption bands observed. Hence, we concluded that excited state linkage thiocyanate isomerization is unlikely to be responsible for the observed transient features.

The second phenomenon that may originate the observed biphasic dynamics is the population of a ^3LF manifold, which may also give rise to distinct spectral signatures. Spectroscopic observation of the ^3LF state has been reported³⁷ when its population is faster than its depletion. In $\{\text{Ru}^{\text{II}}(\text{imine})\}$ complexes this requires a manipulation of the energy levels that results in ^3LF states laying at lower energies than the $^3\text{MLCT}$ states. Hence, ^3LF states get rapidly populated at the expense of the latter and their population is allowed to accumulate and be observed. This was achieved in $[\text{Ru}(\text{bpy})_3]^{2+}$ analogues by ligand functionalization that decreases significantly the energy of the ^3LF states, which in consequence lay below the $^3\text{MLCT}$ states. In the systems reported here, the same energy ordering is obtained by increasing the energy of the $^3\text{MLCT}$ manifold. In **1-2CN** and **1-2NCS**, the $^3\text{MLCT}$ states are at least $\sim 5000 \text{ cm}^{-1}$ higher in energy than in related ruthenium polypyridine complexes based on the energy of the MLCT absorption observed for those complexes. Therefore, the $^3\text{MLCT}$ becomes higher in energy than the ^3LF (as confirmed by the DFT calculations) and as a result of this, a fast population of the ^3LF state is expected. In these complexes the fast conversion to the ^3LF state may allow accumulation of a sufficient concentration of the complex in that state, opening the possibility for its spectroscopic detection.

The spectroscopic signal observed for **ES2** in **1NCS** and **2NCS** is compatible with the expected spectra for ^3LF states. A significant bleach is not anticipated as the

ruthenium ion in the ^3LF state is formally a Ru(II) ion with unpaired electrons in both the t_{2g} and e_g orbitals, and hence MLCT transitions are expected. In addition, the hole in the t_{2g} orbital makes possible LMCT transitions from the NCS^- and the pyridine radical anion ligands. Due to the Ru(II) character of the ^3LF , LMCT transitions are expected at higher energy than in the ground state of $\mathbf{1-2NCS}^+$. The population of ^3LF at the expense of the $^3\text{MLCT}$ should result in the disappearance of the initial ground state bleach and a growth of a photoinduced absorption in the visible, which is observed in the data for $\mathbf{1NCS}$ around 430 nm (Figure 5b). Therefore, we assign the **ES2** as a ^3LF state.

Global fitting analysis of the transient data for $\mathbf{1-2NCS}$ using a parallel five compartment model^{75,76} revealed more spectrally active components than in the case of $\mathbf{1-2CN}$ (Figures S4-7). Hence, a target fit strategy (see Supplementary Information) was followed, using the target model shown in Figure 7. In this model, the $^3\text{MLCT}$ initially created by the pump pulse (**ES1**) either reverts to the ground state (**GS0**), or it populates the intermediate excited state (**ES2**) which then decays to ground state. For both $\mathbf{1NCS}$ and $\mathbf{2NCS}$, kinetic traces (Figures 6 and S9) are well described by this three-state target model. Figures 8 and S8 show the resulting Species Associated Difference Spectra (SADS) for $\mathbf{1NCS}$ and $\mathbf{2NCS}$, respectively, which can be associated with the states proposed in our model.⁷⁵ Table 4 collects the parameters obtained by this procedure. The transition to the ^3LF state in $\mathbf{1NCS}$ and $\mathbf{2NCS}$ is fast ($\tau = 1.67$ and 1.29 ps, respectively), while its decay to ground state is slower, corresponding to 9.7 and 12 ps.

The same model accounts for the kinetic behavior of $\mathbf{1CN}$ and $\mathbf{2CN}$. In this case the energy gap between the $^3\text{MLCT}$ and the ^3LF is smaller due the destabilization induced in ^3LF state by cyanide ligands. This results in a ^3LF manifold with a feeding process slower than its lifetime, so it never reaches a significant concentration and

cannot be spectroscopically detected. As a result, a single exponential decay is observed. It is worth to note that we cannot completely rule out the presence of very low amounts of photoproducts. Given the low quantum yields of photodissociation observed in related complexes, the concentration of these photoproducts is expected to be low, and should not have a major influence in the photophysical behavior described.⁷⁷ Otherwise, additional time constants would have been required for the model to adequately fit our experimental data. Hence, we think the generation of photoproducts from ES2 is a minor pathway and the impact of photodecomposition could be safely left out in our photophysical model.

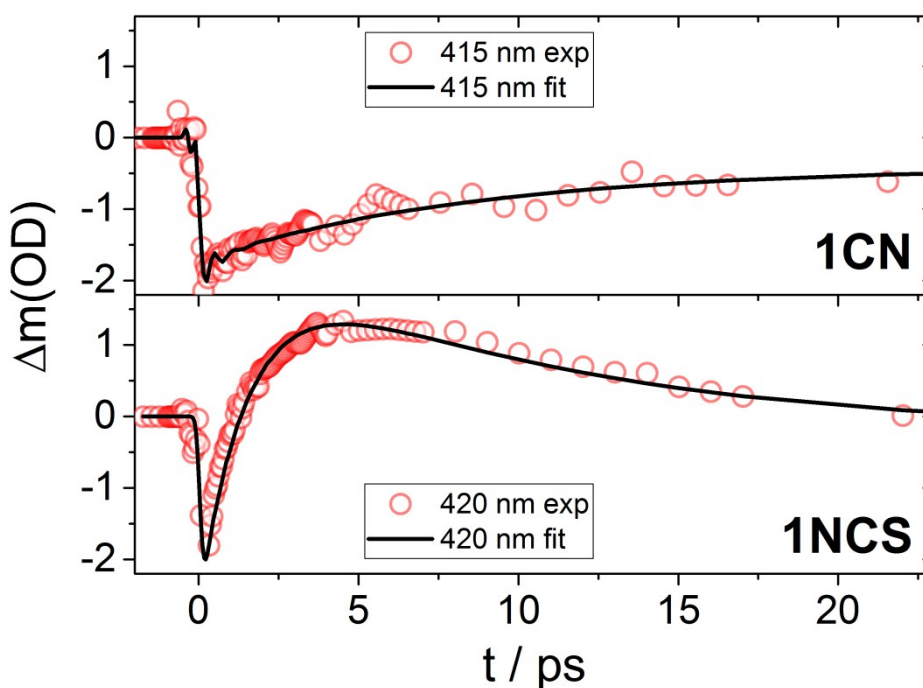


Figure 6. Transient absorption traces of **1CN** and **1NCS** in methanol, pumped at 387 nm. Scatter plots: measured traces. Solid curves: globally fitted functions.

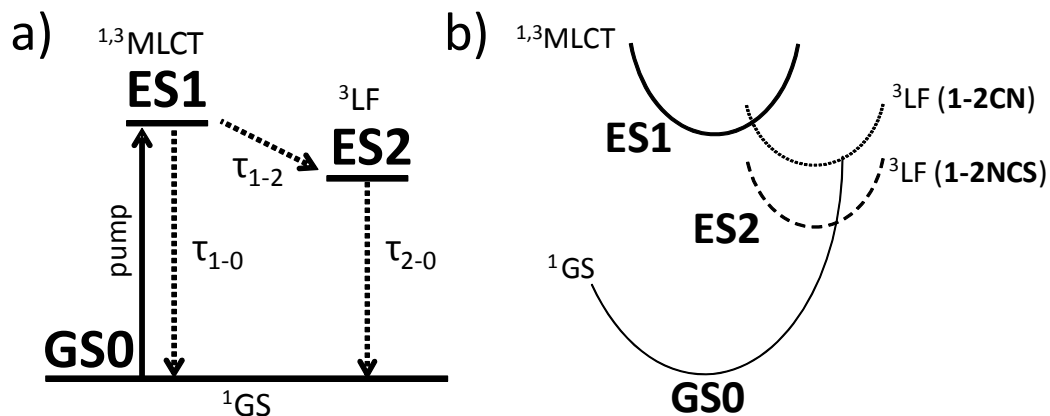


Figure 7. a) Jablonski diagram of the relevant states describing the photophysical behavior of **1-2CN** and **1-2NCS**. The process labeled by τ_{10} corresponds to a radiationless deactivation. b) Potential energy surface diagram illustrating the differences between **1-2CN** and **1-2NCS**.

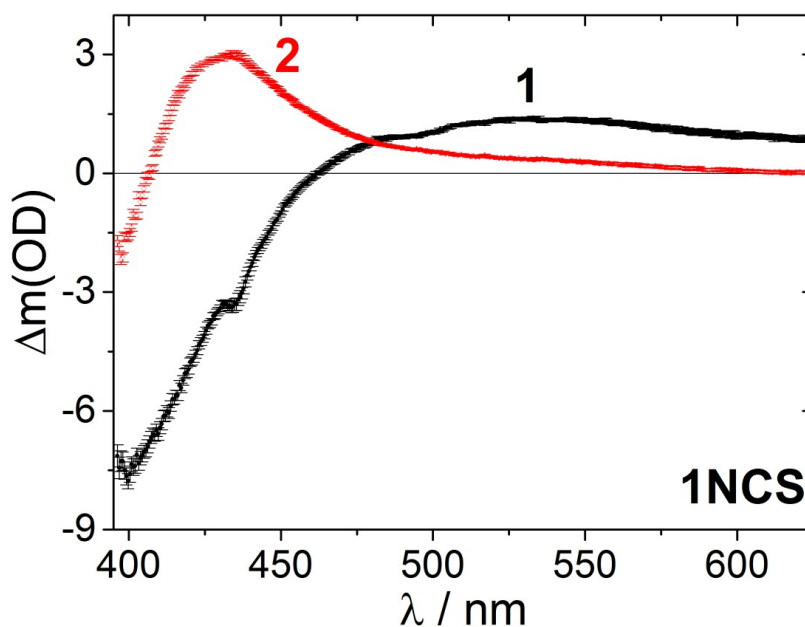


Figure 8. Species Associated Difference Spectra for **1NCS** in MeOH, fitting a three state model as depicted in Figure 7 (Black: state 1, Red: state 2).

Comp.	τ_{10} / ps	τ_{12} / ps	τ_{20} / ps
1CN		8.6 ± 0.2	-
2CN		7.1 ± 0.3	-
1NCS	20 ± 2	1.67 ± 0.01	9.7 ± 0.2

2NCS	26 ± 2	1.29 ± 0.05	12.3 ± 0.2
------	------------	-----------------	----------------

Table 4. Characteristic times of the processes obtained by global fitting of the data to the target model shown in Figure 7.

DFT results

DFT methods were employed to study the structure and spectroscopy of **1-2CN** and **1-2NCS**, and their one-electron oxidized species **1-2CN⁺** and **1-2NCS⁺**. The optimized structures of **1-2CN** and **1-2NCS** agree with the experimentally determined ones (Tables S2 and S3), displaying the typical propeller-like configuration of the {Ru(L)₄} fragments. This geometry is also a characteristic of **1-2CN⁺** and **1-2NCS⁺**.

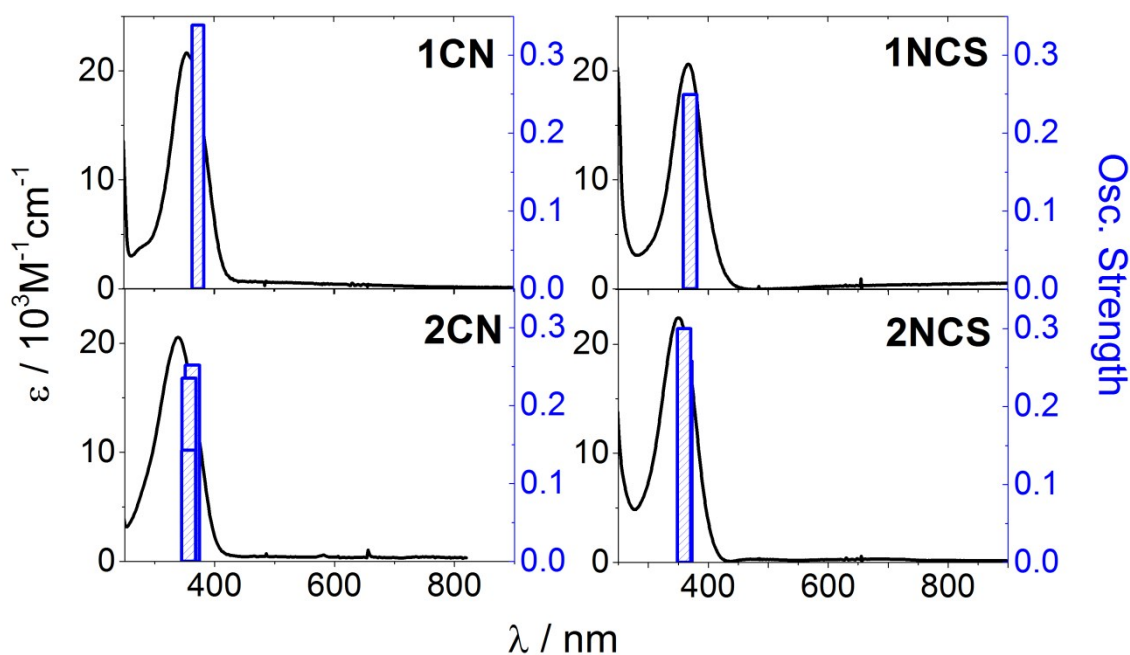


Figure 9. Comparison between the absorption spectra of **1-2CN** and **1-2NCS** (curves) and the energy of the optical transitions predicted by DFT calculations (bars).

As seen in related ruthenium dithiocyanate complexes,^{44,48,52,78–80} in **1-2NCS** the HOMO is metal-based with important contributions (over 35%) of the pseudohalide ligands (Figure S20). Spectroscopy of **1-2CN** and **1-2NCS** predicted by (TD)DFT is in

good agreement with the experimental measurements and supports the assignments made (Figure 9, Tables S4, S6, S8 and S11). It is worth to note at this point that LL'CT $d\pi(\text{SCN}) \rightarrow \pi^*(\text{L})$ transitions are predicted for **1-2NCS** (Tables S14 and S15). Nevertheless, their energy is high enough (over 305 nm) to safely exclude them from the deactivation cascade of MLCT states, so they will be no further discussed. According to our DFT calculations for the one-electron oxidized species **1-2CN⁺** and **1-2NCS⁺**, the computed spin densities (Figure S21) are primarily centered on ruthenium ions, with the hole partially located on NCS⁻ ligands (around 15%) for **1-2NCS⁺**.⁴⁸ This result confirms that the oxidation processes observed in electrochemical experiments (Figure S2 and Table 2) are metal-centered.

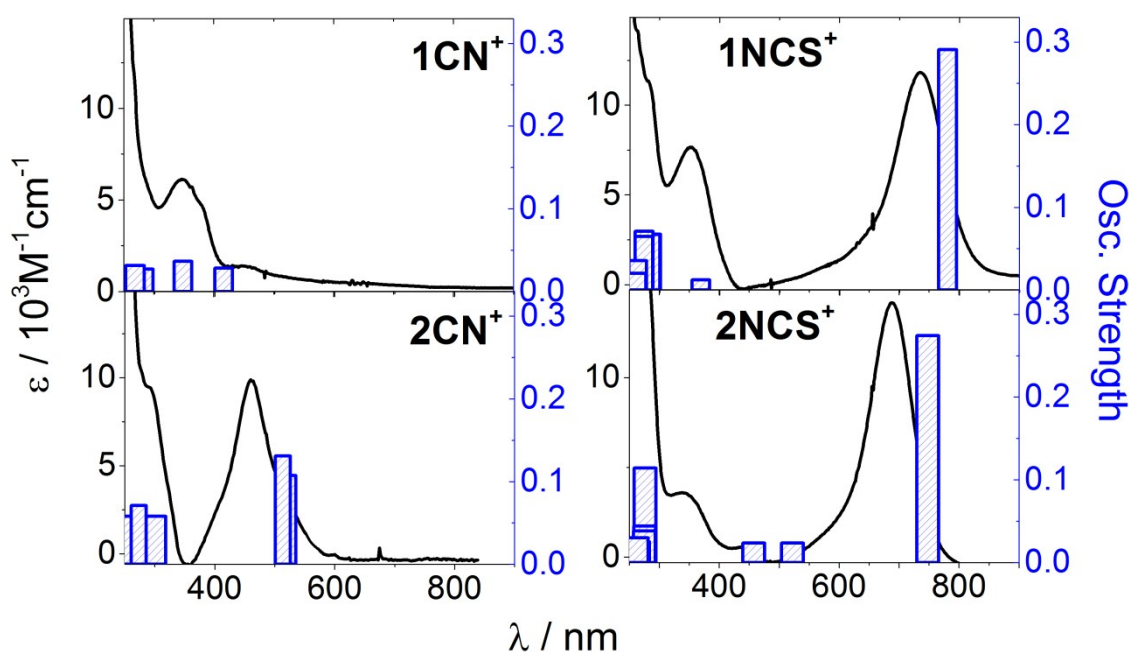


Figure 10. Comparison between the absorption spectra of **1-2CN⁺** and **1-2NCS⁺** (curves) and the energy of the optical transitions predicted by DFT calculations (bars).

Spectroscopic predictions provided by (TD)DFT methods for the transitions in **1-2CN⁺** and **1-2NCS⁺** are also consistent with the experiments (Figure 10, Tables S5,

S7, S9, S12). Importantly, the predicted LMCT bands from pyridinic ligands in **1-2CN**⁺ and from thiocyanates in **1-2NCS**⁺ are very close to those obtained experimentally, and the trends upon pyridine substitution are well reproduced. Further inspection of these bands in **1CN**⁺ reveal contributions of $\pi(\text{CN})$ orbitals to the donor state involved in the transition calculated to be at 349 nm and 448 nm (Table S5, Figure S11), which are absent in **2CN**⁺ (Table S7) and may account for the different intensities experimentally observed when changing the pyridinic ligand. In **1-2NCS**⁺, the high energy LMCT bands can be attributed to $\pi(\text{L}) \rightarrow d\pi(\text{Ru})/\pi(\text{NCS})$ (Tables S9 and S12). Their insensitivity towards pyridine substitution may be due to appreciable contributions of $\pi(\text{NCS})$ components to the LUMO of both **1-2NCS**⁺ (Figures S15 and S18), which reduces the influence of the ruthenium reduction potential on the energy of the transition. These results highlight the good agreement between the DFT descriptions of the electronic structure for our series of compounds with their experimental behavior. This is further demonstrated by the nice correlation between the experimental and the calculated oscillator strengths of the discussed transitions (Table S17 and Figure S26).

With the aim of exploring the properties of the ³LF states **ES2** involved in the decay pathways of **1-2NCS** and **1-2CN**, an optimization of the structures of the lowest-lying electronically excited state with triplet character was performed. The computed spin densities of these states are essentially centered on the ruthenium ion, with values of 1.822 (**1NCS**), 1.931 (**2NCS**), 1.912 (**1CN**) and 1.905 (**1CN**), suggesting that they are of ligand field nature.⁸¹ A corresponding orbital transformation⁸²⁻⁸⁴ was performed on these spin unrestricted computation outputs to elucidate the occupation pattern of the molecular orbitals in these triplets. For all the complexes reported here, this yielded antibonding HOMOs of σ symmetry, and non-bonding (HOMO-1)s of π symmetry (Figures S22-25), consistent with a $(t_{2g})^5(e_g)^1$ electronic configuration in an octahedral

environment. The calculated energy of the ^3LF states suggest they lay closer to the ground state for the NCS^- complexes compared to the complexes containing CN^- , as well as the complexes containing the ligand MeOpy compared to the py complexes (Table S16), although differences are small.

In order to explore the spectroscopy of the ^3LF excited states of **1-2NCS**, (TD)DFT calculations were performed to predict the spectral locus of the electronic transitions arising from them (Tables S10 and S13). A remarkable agreement with the experimental transient absorption spectra at 5 ps was found. Specifically, for **1NCS**, a positive absorption band is observed between 400 and 500 nm, reproduced by expected transitions at 431 nm and 448 nm (Figure 11 and Table 5). The first one corresponds to a $\pi(\text{NCS}) \rightarrow d\pi(\text{Ru})$ LMCT, and the second to a $d\pi(\text{Ru}) \rightarrow \pi^*(\text{py})$ MLCT (Table S10). In the case of **2NCS**, the (TD)DFT calculation provides transitions at 397 nm and 399 nm, matching the experimental red flank of a band with a maximum below 410 nm (Figure 11). Those transitions can be described as $d\pi(\text{Ru}) \rightarrow \pi^*(\text{MeOpy})$ MLCT charge transfers. Furthermore, a $\pi(\text{NCS}) \rightarrow d\pi(\text{Ru})$ LMCT band at 464 nm is also predicted by our (TD)DFT calculations, which contributes to the broad profile of the detected signal (Table S13). The observed agreement between the predicted transitions for the ^3LF excited state of **1-2NCS** and the photoinduced absorptions associated with the intermediate excited state **ES2** in their transient absorption spectroscopy provides further evidence of the ^3LF the nature of those states as assigned above.

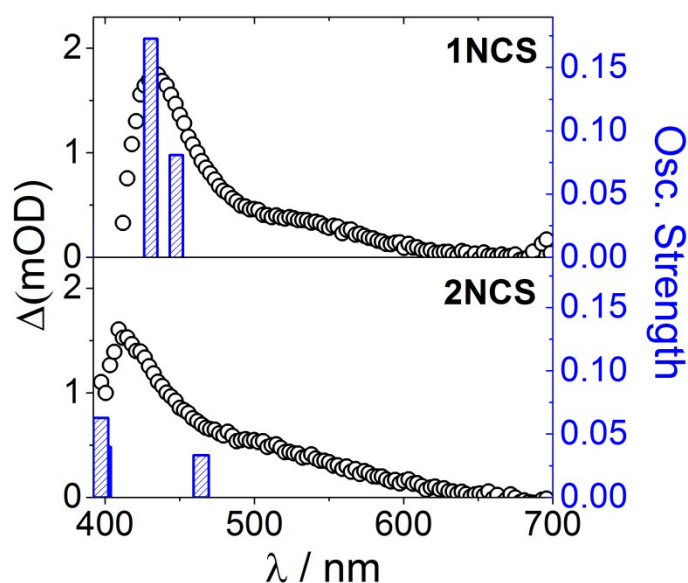


Figure 11. Comparison between the difference absorption spectra of **1-2NCS** 5 ps after the pump pulse (curves) and the energy of the optical transitions predicted for their lowest triplet state by DFT calculations (bars).

Comp.	$\lambda_{\text{exp}} / \text{nm}$	$\lambda_{\text{calc}} / \text{nm}$	Assignment
1NCS	433	431	$\pi(\text{NCS}) \rightarrow d\pi(\text{Ru})$
	nr	448	$d\pi(\text{Ru}) \rightarrow \pi^*(\text{py})$
2NCS	< 410	397	$d\pi(\text{Ru}) \rightarrow \pi^*(\text{MeOpy})$
		399	$d\pi(\text{Ru}) \rightarrow \pi^*(\text{MeOpy})$
		464	$\pi(\text{NCS}) \rightarrow d\pi(\text{Ru})$

Table 5. Comparison between the difference absorption data 5 ps after the pump pulse and the calculated transitions for the lowest triplet state of **1-2NCS**. nr: not resolved.

Discussion

Spectroelectrochemical experiments provided successful approximations to the absorption spectroscopy of the MLCT manifold. The deviations observed are related to the simultaneous presence of a reduced ligand and an oxidized metal center in the excited states. In **1-2NCS**, $X \rightarrow \text{Ru}$ LMCT bands are predicted at longer wavelengths than they are detected by transient absorption experiments, and in **2CN** this shift probably leaves this band out of the experimental window. This difference stems from

the destabilization of the ruthenium orbitals introduced by the reduced pyridinic ligands present in the $^3\text{MLCT}$ state.

An accurate representation of the deactivation cascade of the $^3\text{MLCT}$ manifold of **1-2NCS** requires the participation of an intermediate state of lower energy. Analysis of their spectral features and comparisons to related compounds suggest that this state is the ^3LF manifold. This hypothesis is also supported by (TD)DFT calculations. For these complexes, ^3LF states lay closer to the ground state than the $^3\text{MLCT}$, contrary to what is usually observed in related polypyridine complexes. This is due to the higher energy of the $^3\text{MLCT}$ states in the complexes reported here. This results in a fast transition to the ^3LF manifold, which is substantially populated from the $^3\text{MLCT}$ on a 1.2-1.7 ps time scale through a downhill process. With a 10 ps time constant, the decay of the LF states is slower, allowing their spectroscopic detection. For comparison, the latter decay rate is similar to that reported for the 7.5 ps time constant of the ^3LF state in another ruthenium polypyridine complex.³⁷ It is worth to note that the initial relaxation is most likely to follow a $^1\text{MLCT}$ - $^3\text{MLCT}$ route (known to occur in around 50 fs) rather than a $^1\text{MLCT}$ - ^1MC cascade. This is also supported by DFT calculations which predict that the ^1MC states are higher in energy than the $^1\text{MLCT}$ (Table S18).

In the transient absorption spectroscopy **1CN** and **2CN** only one excited state that we assign as a $^3\text{MLCT}$ state can be observed. This behavior can be accounted by the same mechanism proposed for **1-2NCS**, but with a slower population rate for the ^3LF state. Thus, for **1CN** and **2CN** the ^3LF state never acquires enough population to be detected. Hence the observed decay rate corresponds to the rate of population of the ^3LF , and no information about the decay rate of this state can be obtained from the kinetic traces. The slower population of the ^3LF may be a result of the strong acceptor character of the cyanide ligands that pushes the ^3LF manifold towards higher energies

diminishing the energy gap with the $^3\text{MLCT}$ state (Figure 7b). However, the DFT calculated energies does not show significant differences on the energies of the ^3LF states of dicyano and dithiocyanate complexes. Therefore, the electronic structure may have an impact on the kinetics of the population of the ^3LF state beyond the difference in energy.

The favorable rates of population and decay of the ^3LF in **1NCS** allowed us to observe its spectroscopy which is particularly rich due to the presence of the NCS^- ligand in the coordination sphere of the ruthenium. The spectrum of the ^3LF of **1NCS** as obtained from SADS, is very similar to the observed spectrum after 5 ps of excitation, which shows a strong absorption centered at 430 nm. This feature is probably a superposition of several bands corresponding to LMCT and MLCT transitions in the LF state. The MLCT transitions are expected occur in the ^3LF state because it has a Ru(II) ion, while the LMCT transitions are expected from the presence of a hole in the t_{2g} orbitals. The same transitions are present in **1NCS**⁺, that also presents a hole in the t_{2g} orbital, but very shifted to the red due to the presence of a Ru(III) ion in this redox state. (TD)DFT calculations are in agreement with these assignments as they also predict MLCT and LMCT bands in this region. This illustrates the simultaneous donor and acceptor character of the Ru ion in ^3LF states.

Conclusion

The dynamics of the spectroscopy of complexes **1-2CN** and **1-2NCS** illustrates the impact of the ^3LF states on the lifetime of the initially populated $^3\text{MLCT}$. For the dicyano compounds **1-2CN** the MLCT manifold population quickly decay, probably through the ^3LF although there is no direct evidence of its presence. In contrast, in the dithiocyanate complexes **1-2NCS** we found clear spectroscopic signatures of the

participation of ^3LF states in the $^3\text{MLCT}$ decay cascade and we have been able to identify the spectral signatures for these states. These spectra evidence the dual donor and acceptor nature of the Ru ion in ^3LF states, as (TD)DFT calculations reveal the presence of both MLCT and LMCT transient absorption bands. The observation of the spectrum of the ^3LF state may prove relevant to its identification in other ruthenium-iminic systems, where the ^3LF plays a dominant role in defining their photochemistry.

Experimental Section

Materials

trans-[Ru(py)₄Cl₂],³⁸ *trans*-[Ru(MeOpy)₄Cl₂],⁴³ *trans*-[Ru(py)₄(CN)₂]³⁸ (**1CN**), *trans*-[Ru(MeOpy)₄(CN)₂]⁴¹ (**2CN**), and *trans*-[Ru^{II}(py)₄(NCS)₂]⁴⁰ (**1NCS**) were prepared according to literature procedures. Solvents for electrochemical and spectral measurements were dried using a PureSolv Micro solvent purification system. All other reagents were obtained commercially and used as supplied. The compounds synthesized were dried in a vacuum desiccator for at least 12 hours prior to characterization.

Synthesis of the complexes

trans-[Ru^{II}(4-metoxypyridine)₄(NCS)₂] (**2NCS**). The procedure is analogous to that reported for **2CN**,⁴¹ but replacing KCN with KSCN. Yield: (54%). Anal. Calcd. for **2NCS** (RuC₂₆H₂₈N₆O₄S₂): C, 47.8; H, 4.3; N, 12.9; S, 9.8; Found: C, 47.6; H, 4.3; N, 12.9; S, 9.8. ¹H NMR (200 MHz, MeOD) δ 7.89 (d, 8H, Ha) 6.85 (d, 8H, Hb), 3.87 (s, 12H, Hc).

General Procedures

IR spectra were collected with a Nicolet FTIR 510P instrument, as KBr pellets. UV–visible spectra were recorded with a Hewlett-Packard 8453 diode array spectrometer (range 190–1100 nm). Elemental analyses were carried on a Carlo Erba 1108 analyzer with an estimated error of $\pm 0.5\%$. NMR spectra were taken in a Bruker 200 MHz spectrometer. Electrochemical measurements were performed under argon with millimolar solutions of the compounds, using a TEQ V3 potentiostat and a standard three electrode arrangement consisting of a glassy carbon disc (area = 9.4 mm²) as the working electrode, a platinum wire as the counter electrode and a silver wire as reference electrode plus an internal ferrocene (Fc) standard. Tetra-*n*-butylammonium hexafluorophosphate ([TBA]PF₆, 0.1 M) was used as the supporting electrolyte. All the potentials reported in this work are referenced to the standard Ag/AgCl saturated KCl electrode (0.197 V vs. NHE), the conversions being performed with literature values for the Fc⁺/Fc couple.⁸⁵ All the spectroelectrochemical (SEC) experiments were performed using a three-electrode OTTLE cell,⁸⁶ with millimolar solutions of the compounds using [TBA]PF₆ 0.1 M as the supporting electrolyte. Oxidation processes were accomplished by electrolysis at 1.2 V and reductions at –2.5 V.

Samples for transient absorption (TA) measurements were dissolved in thoroughly argon-degassed anhydrous methanol and placed in a two millimeter pathlength cuvette. Optical densities (OD) were ~1 at excitation wavelengths ($\lambda_{\text{exc}} = 387$ nm). Ultrafast TA experiments were performed with a Clark MXR CPA 2010 laser system employing a fiber-based spectrometer (HELIOS). TA experiments were conducted by exciting samples at 387 nm (3.20 eV) with ~150 fs pulses (pump fluence 50 $\mu\text{J}/\text{cm}^2$). Excitation light was generated using the second harmonic of the fundamental. Transient absorption spectra were subsequently acquired with a delayed,

low-intensity white light continuum with wavelengths between 400 and 700 nm. White light was generated focusing a 5% fraction splitted from the fundamental beam onto a CaF₂ window. Four scans (4000 laser shots) were averaged to obtain each TDA spectrum.

Global analysis was performed with a suggested procedure.⁷⁵ To take into account possible complex photophysics, five time constants were preliminarily proposed, and a SVD strategy was applied to identify the number of spectrally active present components. A Gaussian IRF with a FWHM of 0.25 ps was convoluted with the model. For **1-2NCS**, Target Analysis was performed fitting a three states model, only considering a 400 nm - 610 nm range to avoid noise interference. This rendered the corresponding Species Associated Difference Spectra (SADS). Further details can be found in the Supplementary Information.

X-Ray Structure Determination

Crystal structure of compound **2NCS** was determined with an Oxford Xcalibur, Eos, Gemini CCD area-detector diffractometer using graphite-monochromated Mo-*K* α radiation ($\lambda = 0.71069 \text{ \AA}$) at 298 K. Data was corrected for absorption with CrysAlisPro, Oxford Diffraction Ltd., Version 1.171.33.66, applying an empirical absorption correction using spherical harmonics, implemented in SCALE3 ABSPACK scaling algorithm.⁸⁷ The structure was solved by direct methods with SIR97⁸⁸ and refined by full-matrix least-squares on F^2 with SHELXL-2014⁸⁹ under WinGX platform.⁹⁰ Hydrogen atoms were added geometrically and refined as riding atoms with a uniform value of U_{iso} . Final crystallographic data and values of R_1 and wR are listed in Table S1 while the main angles and distances are listed in Table 1. CCDC 1410384 contains the supplementary crystallographic data for this paper. These data can be obtained free of

charge from the Cambridge Crystallographic Data Center via www.ccdc.cam.ac.uk/data_request/cif.

Theoretical Calculations

We employed Density Functional Theory (DFT) computations to fully optimize the geometries of the two redox states of *trans*-[Ru(L)₄(X)₂] in methanol, without symmetry constraints. For the Ru(II) complexes, both singlet and triplet states geometry optimizations were performed. The calculations were done with the *Gaussian09* package,⁹¹ at the B3LYP level of theory using restricted and unrestricted approximations of the Kohn-Sham equations, depending on the total number of electrons.⁹² In all cases, we employed the effective core potential basis set LanL2DZ, which proved to be suitable for geometry predictions in coordination compounds containing metals of the second row of the transition elements in the Periodic Table. All the calculations were performed using an UltraFine grid. Solvation effects were accounted for using the most recent implementation of the implicit IEF-PCM solvation model.⁹³⁻⁹⁵ We used tight convergence criteria in the geometry optimizations and default settings for IR calculations. All optimized structures were confirmed as minima by analyzing the harmonic vibrational frequencies.⁹⁶ Vertical electronic excitation energies and intensities were evaluated using time-dependent DFT ((TD)-DFT)^{97,98} approach with the *Gaussian09* package,⁹¹ without symmetry constraints and the isodensity plots of the orbitals involved in these transitions were visualized using Molekel.^{99,100} GaussSum¹⁰¹ software was used to perform spectral simulation and to extract spectral data and molecular orbital information. To evaluate the effect of spin contamination, (TD)DFT calculations on the triplet states were performed in two ways, first, starting from the ³LF geometry and its wavefunction and second, by

starting from a singlet closed-shell species at the 3LF geometry. The results obtained with both strategies agreed with each other for all the transitions relevant to the proposed mechanism. The calculated absorption spectra, the composition of electronic transitions, and the associated molecular orbitals for all the calculated complexes are shown in the Supporting Information.

Acknowledgements

The authors acknowledge Prof. Leonardo D. Slep for his guidance with the corresponding orbital transformations, Prof. Pablo Alborés for the crystal structure refinement, Dr. Prashant Kamat for providing access to TA setup, and Dr. Kevin Stamplecoskie for kind assistance. J.H.H and L.B.V. thank the University of Buenos Aires (UBACYT Q643), the Consejo Nacional de Investigaciones Científicas y Técnicas (CONICET) and the Agencia Nacional de Promoción Científica y Tecnológica (PICT 2012-2041) for funding. J.H.H and L.B.V. are members of the scientific staff of CONICET; A.C. and G.E.P. are postdoctoral fellows of the same institution. M.K. thanks the National Science Foundation (Grant No. CHE1208091) for financial support of this study. P.T. thanks the Royal Thai Government Scholarship Program for financial support. A.C. acknowledges ALN for discussions on basic topics. G.E.P. thanks Prof. Adrián Roitberg for selflessly sharing his knowledge.

Notes and References

- (1) Castellano, F. N. *Acc. Chem. Res.* **2015**, *48*, 828–839.
- (2) Hammarström, L. *Acc. Chem. Res.* **2015**, *48*, 840–850.
- (3) Morseth, Z. a.; Wang, L.; Puodziukynaite, E.; Leem, G.; Gilligan, A. T.; Meyer, T. J.; Schanze, K. S.; Reynolds, J. R.; Papanikolas, J. M. *Acc. Chem. Res.* **2015**, *48*, 818–827.

- (4) Gu, J.; Yan, Y.; Helbig, B. J.; Huang, Z.; Lian, T.; Schmechl, R. H. *Coord. Chem. Rev.* **2015**, 282-283, 100–109.
- (5) Zeitler, K. *Angew. Chemie Int. Ed. English* **2009**, 48, 9785–9789.
- (6) Dürr, H.; Bossmann, S. *Acc. Chem. Res.* **2001**, 34, 905–917.
- (7) Alibabaei, L.; Sherman, B. D.; Norris, M. R.; Brennaman, M. K.; Meyer, T. J. *Proc. Natl. Acad. Sci.* **2015**, 112, 5899–5902.
- (8) Sander, A. C.; Maji, S.; Francàs, L.; Böhnisch, T.; Dechert, S.; Llobet, A.; Meyer, F. *ChemSusChem* **2015**, 8, 1697–1702.
- (9) Wang, L.; Mirmohades, M.; Brown, A.; Duan, L.; Li, F.; Daniel, Q.; Lomoth, R.; Sun, L.; Hammarström, L. *Inorg. Chem.* **2015**, 54, 2742–2751.
- (10) Sala, X.; Maji, S.; Bofill, R.; García-Antón, J.; Escriche, L.; Llobet, A. *Acc. Chem. Res.* **2014**, 47, 504–516.
- (11) Odobel, F.; Pellegrin, Y.; Warnan, J. *Energy Environ. Sci.* **2013**, 6, 2041.
- (12) Bignozzi, C. A.; Argazzi, R.; Boaretto, R.; Busatto, E.; Carli, S.; Ronconi, F.; Caramori, S. *Coord. Chem. Rev.* **2012**, 257, 1472–1492.
- (13) Polo, A. S.; Itokazu, M. K.; Murakami Iha, N. Y. *Coord. Chem. Rev.* **2004**, 248, 1343–1361.
- (14) Ardo, S.; Meyer, G. *Chem. Soc. Rev.* **2009**, 38, 115–164.
- (15) Hagfeldt, A.; Boschloo, G.; Sun, L.; Kloo, L.; Pettersson, H. *Chem. Rev.* **2010**, 110, 6595–6663.
- (16) Grätzel, M. *Nature* **2001**, 414, 338–344.
- (17) Yue, X.; Zhu, Z.; Zhang, M.; Ye, Z. *Anal. Chem.* **2015**, 87, 1839–1845.
- (18) Zheng, Z.-B.; Wu, Y.-Q.; Wang, K.-Z.; Li, F. *Dalt. Trans.* **2013**, 43, 3273–3284.
- (19) Rice, C. R.; Guerrero, A.; Bell, Z. R.; Paul, R. L.; Motson, G. R.; Jeffery, J. C.; Ward, M. D. *New J. Chem.* **2001**, 25, 185–187.
- (20) Anzenbacher, P.; Tyson, D. S.; Jursíková, K.; Castellano, F. N. *J. Am. Chem. Soc.* **2002**, 124, 6232–6233.
- (21) Keefe, M.; Benkstein, K. D.; Hupp, J. T. *Coord. Chem. Rev.* **2000**, 205, 201–228.
- (22) Zayat, L.; Calero, C.; Alborés, P.; Baraldo, L.; Etchenique, R. *J. Am. Chem. Soc.* **2003**, 125, 882–883.
- (23) Nikolenko, V.; Yuste, R.; Zayat, L.; Baraldo, L. M.; Etchenique, R. *Chem. Commun.* **2005**, 1752–1754.
- (24) Campagna, S.; Puntoriero, F.; Nastasi, F.; Bergamini, G.; Balzani, V. *Top. Curr. Chem.* **2007**, 280, 117–214.
- (25) Juris, A.; Balzani, V.; Barigeletti, F.; Campagna, S.; Belser, P.; von Zelewsky, A. *Coord. Chem. Rev.* **1988**, 84, 85–277.
- (26) McCusker, J. K. *Acc. Chem. Res.* **2003**, 36, 876–887.
- (27) Hammarström, L.; Johansson, O. *Coord. Chem. Rev.* **2010**, 254, 2546–2559.

- (28) Dixon, I. M.; Lebon, E.; Sutra, P.; Igau, A. *Chem. Soc. Rev.* **2009**, *38*, 1621–1634.
- (29) Sun, Q.; Mosquera-vazquez, S.; Suffren, Y.; Hankache, J.; Amstutz, N.; Max, L.; Daku, L.; Vauthey, E.; Hauser, A. *Coord. Chem. Rev.* **2015**, *283*, 87–99.
- (30) Xia, H.; Liu, F.; Ardo, S.; Narducci, A. A.; Meyer, G. J. *J. Photochem. Photobiol. A Chem.* **2010**, *216*, 94–103.
- (31) Van Houten, J.; Watts, R. J. *J. Am. Chem. Soc.* **1976**, *98*, 4853–4858.
- (32) Welby, C. E.; Rice, C. R.; Elliott, P. I. P. *Angew. Chemie Int. Ed. English* **2013**, *52*, 1–5.
- (33) Wagenknecht, P. S.; Ford, P. C. *Coord. Chem. Rev.* **2011**, *255*, 591–616.
- (34) Carrone, G.; Etchenique, R. *Anal. Chem.* **2015**, *87*, 4363–4369.
- (35) Zayat, L.; Filevich, O.; Baraldo, L. M.; Etchenique, R. *Philos. Trans. A. Math. Phys. Eng. Sci.* **2013**, *371*, 1–12.
- (36) Hewitt, J. T.; Vallett, P. J.; Damrauer, N. H. *J. Phys. Chem. A* **2012**, *116*, 11536–11547.
- (37) Sun, Q.; Mosquera-Vazquez, S.; Lawson Daku, L. M.; Guénée, L.; Goodwin, H. A.; Vauthey, E.; Hauser, A. *J. Am. Chem. Soc.* **2013**, *135*, 13660–13663.
- (38) Coe, B. J.; Meyer, T. J.; White, P. S. *Inorg. Chem.* **1995**, *34*, 3600–3609.
- (39) Coe, B. J.; Meyer, T. J.; White, P. S. *Inorg. Chem.* **1995**, *34*, 593–602.
- (40) Chen, J.; Han, L.; Chen, Z. *Acta Crystallogr. Sect. E Struct. Reports Online* **2002**, *58*, m588–m589.
- (41) Pieslinger, G. E.; Albores, P.; Slep, L. D.; Coe, B. J.; Timpson, C. J.; Baraldo, L. M. *Inorg. Chem.* **2013**, *52*, 2906–2917.
- (42) Cadranel, A.; Hodak, J. H. *J. Coord. Chem.* **2015**, *68*, 1452–1464.
- (43) Alborés, P.; Slep, L. D.; Weyhermüller, T.; Baraldo, L. *Inorg. Chem.* **2004**, *43*, 6762–6773.
- (44) Cecchet, F.; Gioacchini, A. M.; Marcaccio, M.; Paolucci, F.; Roffia, S.; Alebbi, M.; Bignozzi, C. A. *J. Phys. Chem. B* **2002**, *106*, 3926–3932.
- (45) Wolfbauer, G.; Bond, A. M.; MacFarlane, D. R. *Inorg. Chem.* **1999**, *38*, 3836–3846.
- (46) Bond, A. M. *J. Electrochem. Soc.* **1999**, *146*, 648–656.
- (47) Wiberg, K. B.; Lewis, T. P. *J. Am. Chem. Soc.* **1970**, *1635*, 7154–7160.
- (48) Kämper, S.; Paretzki, A.; Fiedler, J.; Záliš, S.; Kaim, W. *Inorg. Chem.* **2012**, *51*, 2097–2104.
- (49) Wang, Q.; Zakeeruddin, S. M.; Nazeeruddin, M. K.; Humphry-Baker, R.; Grätzel, M. *J. Am. Chem. Soc.* **2006**, *128*, 4446–4452.
- (50) Tachibana, Y.; Moser, J.-E. E.; Grätzel, M.; Klug, D. R.; Durrant, J. R.; Grätzel, M.; Klug, D. R.; Durrant, J. R. *J. Phys. Chem.* **1996**, *100*, 20056–20062.
- (51) Moser, J. E.; Noukakis, D.; Bach, U.; Tachibana, Y.; Klug, D. R.; Durrant, J. R.;

- Humphry-baker, R.; Gratzel, M. *J. Phys. Chem. B* **1998**, *102*, 3649–3650.
- (52) Li, X.; Nazeeruddin, M. K.; Thelakkat, M.; Barnes, P. R. F.; Vilar, R.; Durrant, J. R. *J. Phys. Chem. Chem. Phys.* **2011**, *13*, 1575–1584.
- (53) Brown, A. M.; McCusker, C. E.; McCusker, J. K. *Dalt. Trans.* **2014**, *43*, 17635–17646.
- (54) Maestri N Balzani, V Constable, Ec Thompson, Amwc, M. A. *Inorg. Chem.* **1995**, *34*, 2767.
- (55) Anderson, P. A.; Keene, F. R.; Meyer, T. J.; Moss, J. A.; Strouse, G. F.; Treadway, J. A. *J. Chem. Soc. Dalt. Trans.* **2002**, 3820–3831.
- (56) Curtright, A. E.; McCusker, J. K. *J. Phys. Chem. A* **1999**, *103*, 7032–7041.
- (57) Damrauer, N. H.; McCusker, J. K. *J. Phys. Chem. A* **1999**, *103*, 8440–8446.
- (58) Damrauer, N.; Cerullo, G.; Yeh, A.; Boussie, T.; Shank, C.; McCusker, J. *Science (80-.)*. **1997**, *275*, 54–57.
- (59) Bhasikuttan, A. C.; Suzuki, M.; Nakashima, S.; Okada, T. *J. Am. Chem. Soc.* **2002**, *124*, 8398–8405.
- (60) Braterman, P. S.; Song, J.-I.; Peacock, R. D. *Spectrochim. Acta* **1992**, *48A*, 899–903.
- (61) Berger, R. M.; McMillin, D. R. *Inorg. Chem.* **1988**, *27*, 4245–4249.
- (62) Sun, Y.; Liu, Y.; Turro, C. *J. Am. Chem. Soc.* **2010**, *132*, 5594–5595.
- (63) Indelli, M. T.; Orlandi, M.; Chiorboli, C.; Ravaglia, M.; Scandola, F.; Lafalet, F.; Welter, S.; De Cola, L. *J. Phys. Chem. A* **2012**, *116*, 119–131.
- (64) Herrero, C.; Quaranta, A.; Fallahpour, R.; Leibl, W.; Aukauloo, A. *J. Phys. Chem. C* **2013**, *112*, 9605–9612.
- (65) McClure, B. A.; Rack, J. J. *Eur. J. Inorg. Chem.* **2010**, *2010*, 3895–3904.
- (66) McClure, B. A.; Abrams, E. R.; Rack, J. J. *J. Am. Chem. Soc.* **2010**, *132*, 5428–5436.
- (67) Garg, K.; Engle, J. T.; Ziegler, C. J.; Rack, J. J. *Chemistry* **2013**, *19*, 11686–11695.
- (68) Göttle, A. J.; Alary, F.; Dixon, I. M.; Heully, J.; Boggio-pasqua, M. *Inorg. Chem.* **2014**, *2*, 6752–6760.
- (69) Lutterman, D. A.; Rachford, A. A.; Rack, J. J.; Turro, C. *J. Phys. Chem. Lett.* **2010**, *1*, 3371–3375.
- (70) Lutterman, D. A.; Rachford, A. A.; Rack, J. J.; Turro, C. *J. Phys. Chem. A* **2009**, *113*, 11002–11006.
- (71) Rack, J. J. *Coord. Chem. Rev.* **2009**, *253*, 78–85.
- (72) Li, H.; Zhang, L.; Ye, M.; Fan, X. *Eur. J. Inorg. Chem.* **2015**, *2015*, 5074–5080.
- (73) Compton, R.; Gerardi, H. K.; Weidinger, D.; Brown, D. J.; Dressick, W. J.; Heilweil, E. J.; Owrutsky, J. C. *Chem. Phys.* **2013**, *422*, 135–142.
- (74) O'Donnell, R. M.; Johansson, P. G.; Abrahamsson, M.; Meyer, G. J. *Inorg.*

- Chem.* **2013**, *52*, 6839–6848.
- (75) Van Stokkum, I. H. M.; Larsen, D. S.; Van Grondelle, R. *Biochim. Biophys. Acta - Bioenerg.* **2004**, *1657*, 82–104.
- (76) Mullen, K. M.; van Stokkum, I. H. M. *J. Stat. Softw.* **2007**, *18*, 46.
- (77) Marcolongo, J. P.; Weyhermüller, T.; Slep, L. D. *Inorganica Chim. Acta* **2015**, *429*, 174–182.
- (78) Barpuzary, D.; Banik, A.; Panda, A. N.; Qureshi, M. *J. Phys. Chem. C* **2015**, *119*, 3892–3902.
- (79) Li, M.-X.; Zhang, H.-X.; Zhou, X.; Pan, Q.-J.; Fu, H.-G.; Sun, C.-C. *Eur. J. Inorg. Chem.* **2007**, *2007*, 2171–2180.
- (80) Zedler, L.; Guthmuller, J.; Rabelo de Moraes, I.; Krieck, S.; Schmitt, M.; Popp, J.; Dietzek, B.; Dietzek, B. *J. Phys. Chem. C* **2013**.
- (81) Alary, F.; Heully, J.-L.; Bijeire, L.; Vicendo, P. *Inorg. Chem.* **2007**, *46*, 3154–3165.
- (82) Amos, A. T.; Hall, G. G. *Proc. R. Soc. A, Math. Phys. Eng. Sci.* **1961**, *263*, 483–493.
- (83) Neese, F. *J. Phys. Chem. Solids* **2004**, *65*, 781–785.
- (84) King, H. F.; Stanton, R. E.; Kim, H.; Wyatt, R. E.; Parr, R. G. *J. Chem. Phys.* **1967**, *47*, 1936–1940.
- (85) Noviadri, I.; Brown, K. N.; Fleming, D. S.; Gulyas, P. T.; Lay, P. A.; Masters, A. F.; Phillips, L. *J. Phys. Chem. B* **1999**, *103*, 6713–6722.
- (86) Kaim, W.; Fiedler, J. *Chem. Soc. Rev.* **2009**, *38*, 3373–3382.
- (87) SCALE3 ABSPACK: Empirical absorption correction, CrysAlis – Software package, Oxford Diffraction Ltd., Oxford, 2006.
- (88) Altomare, A.; Burla, M. C.; Camalli, M.; Casciarano, G. L.; Giacovazzo, C.; Guagliardi, A.; Moliterni, A. G.; Polidori, G.; Spagna, R. *J. Appl. Crystallogr.* **1999**, *32*, 115–119.
- (89) Sheldrick, G. M. *Acta Crystallogr. Sect. A Found. Crystallogr.* **2007**, *64*, 112–122.
- (90) Farrugia, L. J. *J. Appl. Crystallogr.* **2012**, *45*, 849–854.
- (91) Gaussian 09, Revision D.01,
M. J. Frisch, G. W. Trucks, H. B. Schlegel, G. E. Scuseria,
M. A. Robb, J. R. Cheeseman, G. Scalmani, V. Barone, B. Mennucci,
G. A. Petersson, H. Nakatsuji, M. Caricato, X. Li, H. P. Hratchian,
A. F. Izmaylov, J. Bloino, G. Zheng, J. L. Sonnenberg, M. Hada,
M. Ehara, K. Toyota, R. Fukuda, J. Hasegawa, M. Ishida, T. Nakajima,
Y. Honda, O. Kitao, H. Nakai, T. Vreven, J. A. Montgomery, Jr.,
J. E. Peralta, F. Ogliaro, M. Bearpark, J. J. Heyd, E. Brothers,

K. N. Kudin, V. N. Staroverov, T. Keith, R. Kobayashi, J. Normand, K. Raghavachari, A. Rendell, J. C. Burant, S. S. Iyengar, J. Tomasi, M. Cossi, N. Rega, J. M. Millam, M. Klene, J. E. Knox, J. B. Cross, V. Bakken, C. Adamo, J. Jaramillo, R. Gomperts, R. E. Stratmann, O. Yazyev, A. J. Austin, R. Cammi, C. Pomelli, J. W. Ochterski, R. L. Martin, K. Morokuma, V. G. Zakrzewski, G. A. Voth, P. Salvador, J. J. Dannenberg, S. Dapprich, A. D. Daniels, O. Farkas, J. B. Foresman, J. V. Ortiz, J. Cioslowski, and D. J. Fox, Gaussian, Inc., Wallingford CT, 2013.

- (92) Szabo, A.; Ostlund, N. S. *Modern Quantum Chemistry: Introduction to Advanced Electronic Structure Theory*; McGraw-Hill, Ed.; New York, 1989.
- (93) Scalmani, G.; Frisch, M. J. *J. Chem. Phys.* **2010**, *132*, 1–15.
- (94) Tomasi, J.; Mennucci, B.; Cammi, R. *Chem. Rev.* **2005**, *105*, 2999–3093.
- (95) Miertuš, S.; Scrocco, E.; Tomasi, J. *Chem. Phys.* **1981**, *55*, 117–129.
- (96) Schlegel, H. B. *J. Comput. Chem.* **1982**, *3*, 214–218.
- (97) Petit, L.; Maldivi, P.; Adamo, C. *J. Chem. Theory Comput.* **2005**, *1*, 953–962.
- (98) Stratmann, R. E.; Scuseria, G. E.; Frisch, M. J. *J. Chem. Phys.* **1998**, *109*, 8218–8224.
- (99) Flükiger, P.; Lüthi, H. P.; Portmann, S.; Weber, J. MOLEKEL 4.3.
- (100) Portmann, S.; Lüthi, H. P. *Chimia (Aarau)*. **2000**, *54*, 766–770.
- (101) O’Boyle, N. M.; Tenderholt, A. L.; Langner, K. M. *J. Comput. Chem.* **2008**, *29*, 839–845.

TOC: Spectroscopic signatures of ligand field states in $\{\text{Ru}^{\text{II}}(\text{imine})\}$ complexes

Clear spectroscopic signatures of ligand field states in the MLCT decay cascade of *trans*- $[\text{Ru}(\text{L})_4(\text{NCS})_2]$ (L = pyridine or 4-methoxypyridine) were found. (TD)DFT calculations reveal the presence of both MLCT and LMCT transient absorption bands, illustrating the simultaneous donor and acceptor character of the Ru ion in LF states.

